# ASTEMA: Design and preliminary performance assessment of a novel tele-microsurgery system

L Vanthournhout, J Szewczyk, J Duisit, B Lengelé, B Raucent, B Herman

# ASTEMA: Design and preliminary performance assessment of a novel tele-microsurgery system

**L. Vanthournhout** [*] **J. Szewczyk** [**] **J. Duisit** [***] **B. Lengelé** [***]
**B. Raucent** [*] **B. Herman** [*]

[*] *Center for Research in Mechatronics, Institute of Mechanics, Materials, and Civil Engineering, Université catholique de Louvain, Louvain-la-Neuve, Belgium, and Louvain Bionics, Université catholique de Louvain (e-mail: lena.vanthournhout@uclouvain.be).*
[**] *Institut des Systèmes Intelligents et de Robotique, Sorbonne Université – Centre National de la Recherche Scientifique, Paris, France (e-mail: szewczyk@isir.upmc.fr)*
[***] *Morphology Research Group, Institute of Experimental and Clinical Research, Université catholique de Louvain, Bruxelles, Belgium, and Department of Plastic and Reconstructive Surgery, Cliniques universitaires Saint-Luc, Université catholique de Louvain, Bruxelles, Belgium (jerome.duisit@uclouvain.be).*

**Abstract:** To fulfill the needs of reconstructive microsurgeons, a teleoperated robot called ASTEMA was built to help surgeons to perform microanastomoses. The surgeon's need is first analysed then the step of the design are presented. This robot is composed of three orthogonal linear actuators and a spherical wrist with its remote center-of-motion at the instrument tip. Geometric model of the spherical wrist was calibrated through mathematical optimization in order to compensate for imperfections of machining and assembling.
Two preliminary experiments were carried out to assess the ASTEMA performance. The first is realized with a simple trajectory in position, a circular trajectory. The second is realized with a complex angular trajectory. They show a significant improvement of gesture precision with respect to manual trajectory execution. They also shows that subjects instinctively compensate the errors from the non-ideal wrist.

*Keywords:* telerobotics, microsurgery, medical devices, design methodology

## 1. INTRODUCTION

Microanastomosis is a microsurgical act that consists in stitching together two very small blood vessels so as to restore blood circulation. This gesture is performed under a microscope as shown in figure 1. It is used in several delicate reconstructive surgery procedures requiring distant tissue transfer like face allograft, torn member saving, finger replantation and cancer reconstruction. In particular, the free flap transfer consists in removing a flap of skin and fat tissue with at least one vein and one artery, and to transfer it to another place on the patient. This procedure requires both speed, to avoid necrosis of the removed graft, and high accuracy to perform an efficient micro-anastomosis and restore blood flow in the graft.

An example of reconstructive surgery is breast reconstruction by DIEP (Deep Inferior Epigastric Perforator) after an ablation due to a cancer. In this surgical operation, the microsurgeon raises a flap from the abdominal wall and grafts it in place of the removed breast. In current practice, the surgeon performing a DIEP flap procedure has to split the pectoralis major and remove a piece of rib, in order to reach the internal thoracic vessels large enough to perform anastomosis safely. Decreasing invasiveness requires using vessels closer to the skin, called « perforator » vessels, with an outer diameter below one millimeter. This makes anastomoses challenging, mainly because of the surgeon's tremor whose magnitude becomes crippling at this scale as shown in figure 2. This physiological limitation prevents the vast majority of microsurgeons to reach such super-microsurgery skills.

Facilitating the surgeon's gestures through a robotic system would decrease both complexity and invasiveness of these procedures, by making anastomoses easier on tiny subsurface blood vessels.

To reduce the surgeon's tremor and increasing gestures accuracy, a teleoperated systems seems a good solution. Most of the existing teleoperated surgical systems are dedicated to minimally invasive keyhole surgery. Among other interesting characteristics for assistance to surgery, these systems allow scaling down the surgeon's gestures,

⋆ This work was supported by F.R.S.-FNRS grant J.0240.16, by UCLouvain FSR grant and own funds from Louvain Bionics (UCLouvain) and UCLouvain.

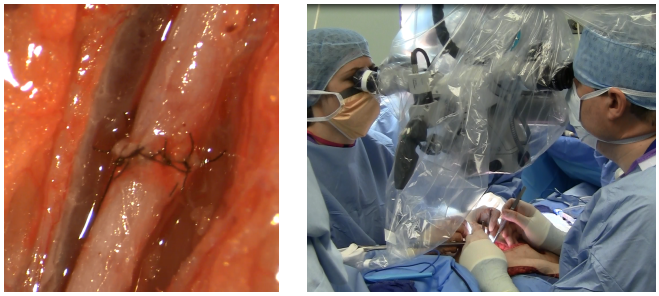

Fig. 1. On left: Microanastomosis with a 1.2 mm diameter vessel. On right: microsurgeons during a DIEP operation.

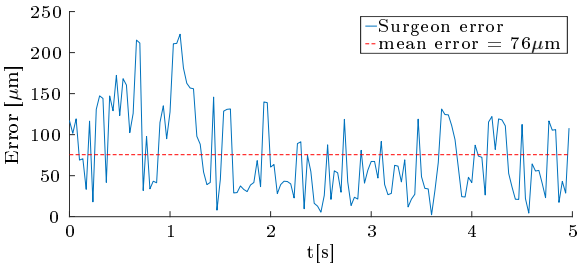


Fig. 2. Surgeon tremor when trying to keep an instrument stationary under a microscope (acquisition at 30 Hz, resolution 6.5 $\mu$m/px, optical magnification x40)

filtering his/her movements and reducing unintentional tremor.

Some studies have demonstrated feasibility and interest of telerobotic assistance to perform microanastomoses with the commercialized Da Vinci system (Intuitive Surgical, Inc.) [Katz et al. (2005); Liverneaux et al. (2013)]. However, general motion accuracy and instruments size are limiting factors to perform supermicrosurgery with this robot [Katz et al. (2005); Taleb et al. (2008)]. Moreover, the Da Vinci system is cumbersome and difficult to introduce or remove from the operating workflow. The later constitutes an important limitation as, usually, microanastomosis is only part of a longer operation that combines acts of normal surgery and microsurgery.

The RAMS workstation from Jet Propulsion Laboratory [Le Roux et al. (2001)] and a recent master-slave system named MSR from spin-off Microsure [Cau (2014)] are microsurgery assistants with higher precision and smaller bulkiness than the Da vinci system, but up to now they double the operation time because of interface limitations [Mitsuishi et al. (2013); Saraf (2008); van Mulken et al. (2018a)]. Other robots were also proposed for teleoperated microsurgery. For example, the telemicrosurgery system developed at Tokyo university for open neurosurgery [Mitsuishi et al. (2013)] or the Robotol system developed at University of Paris VI for middle ear surgery [Miroir et al. (2012)]. However, most of them show the same drawbacks as the Da Vinci or are devoted to specific surgical specialties for which microanastomosis is not a major issue.

In this context, the ASTEMA, Adaptive Scaling TEleMicrosurgery Assistance, is a teleoperated robot dedicated to microanastomosis whose purpose is to increase accuracy and dexterity of the surgeon while limiting the increase in operating time. Its resolution, its size, its workspace, its speed are consistent with the specific requirements of the microanastomosis context.

This paper focuses on the design process of the ASTEMA robot. First, it presents the needs analysis made with the help of several microsurgeons. Then it details the implementation of the robot. Finally, it describes and analyses the first experiments showing that the required specifications are fulfilled.

## 2. NEEDS ANALYSIS

To ensure a good matching between the ASTEMA system and the surgeons' requirements, a needs analysis was carried out based on quantification of gestures and discussion with microsurgeons. The main technical requirements associated to microanastomosis are: speed of gesture, accuracy, dexterity, force capacity and ability to change instrument rapidly.

### *2.1 Instrument workspace*

The surgeon movements during a microanastomosis on a 2 mm diameter vessel from a rat were analyzed and quantified using a set of visual markers and a 3D camcorder. The instrument workspace for instrument tip position is encompassed into a cuboid of 40x50x40 $mm^3$ as shown in the left of the figure 3. The workspace for instrument orientation is included into a cone of 87° as shown in the right of the figure 3, and an instrument self-rotation of more than 360° is exploited. Experiment details can be found in [Vanthournhout et al. (2015a)].

### *2.2 Accuracy*

The required accuracy is not identical during the entire procedure. The microanastomosis procedure can be broken down into several steps: clamp handling (to close the vessel during the procedure), vessel preparation, stitches with needle insertion and knots. Not all steps need the same accuracy. The most difficult gesture is needle insertion because of the size of the vessel and the importance of insertion position for the impermeability of the anastomosis, to avoid stenosis and clotting. Figure 2 shows the tremor of a surgeon who tries to keep an instrument tip steady above a target. The surgeon's usual tremor amplitude is around 100 $\mu$m with a frequency between 6 and 15 Hz [Veluvolu and Ang (2010); Safwat et al. (2009)] while authors estimate the required precision is around 10 $\mu$m for microanastomosis (1% of circle circumference with 0.3 mm diameter).

Very fine gestures like needle insertion need only small angular displacements (around 15 to 20°) with a high accuracy. But gestures like making a knot need large angular displacements with only the human precision around 100$\mu$m.

### *2.3 Rapidity*

The operation duration is also important because if the flap is not revascularised fast enough, the risk of ischemia-related complications such as necrosis becomes significant [Shaw et al. (1996)]. Moreover, the longer the patient is anaesthetized, the higher the risk of complications.

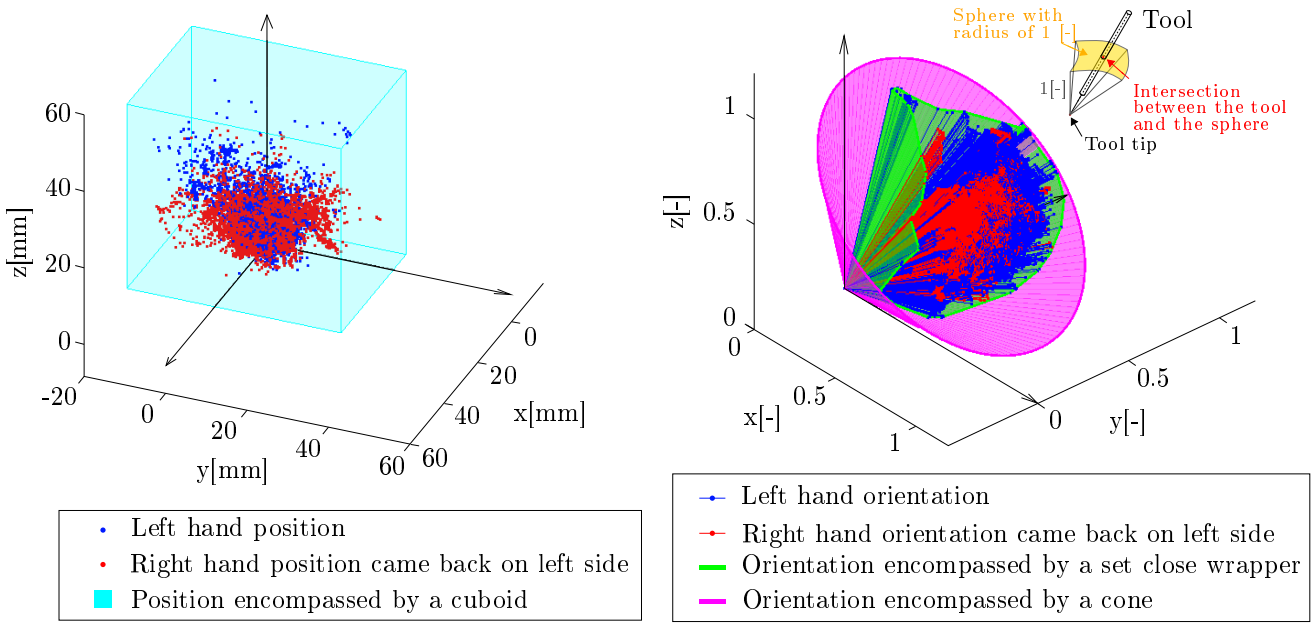


Fig. 3. Microanastomosis workspace realised by a microsurgeon (left-handed person) on a rat. The vessel is on the y-axis. On left: instrument tip position. On right: instrument orientation. The angular position is represented by points which correspond to the intersection between a sphere center on the instrument tip with a dimensionless radius of 1 and the instrument. Adapted from [Vanthournhout et al. (2015a)].

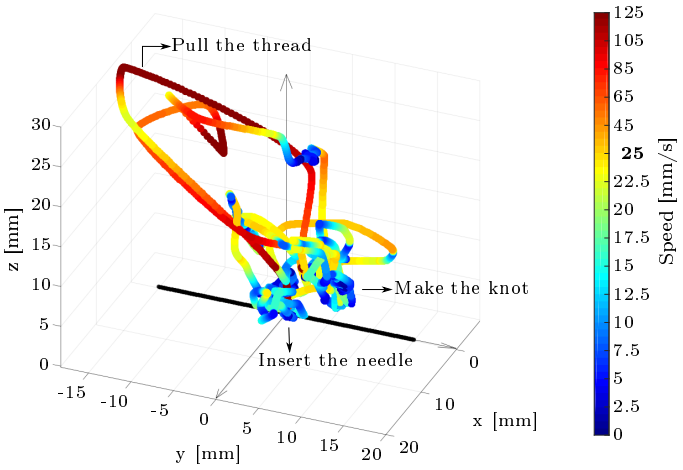


Fig. 4. Speed of surgeon main-hand according position during one stitch and a knot.

Figure 4 shows the speed of gesture during a stitch according to the position. These data come from the workspace experiment. The area close to the vessel, where the surgeon inserts the needle, is where gestures are slow (≤25 mm/s) and is associated with the higher required accuracy. In contrast, when the instrument tip is far from the vessel (e.g. to pull the thread), velocity rises (up to 130 mm/s) and precision is less important. An intermediate area, where the surgeon makes the knots, shows a mix between slow and moderate speed (≤50 mm/s).

### *2.4 Force capacity*

To insert a needle, the force varies between 30 and 50 mN [Mitsuishi et al. (1997)]. It is often so low that the surgeon can hardly feel it [Panchulidze et al. (2011)]. Currently, the surgeon gauges the applied force from visual feedback of the tissue deformation. The clamping force is around 10 to 80 mN to hold a blood vessel and 1 to 2 N to hold a needle or a thread [Mitsuishi et al. (1997)]. Here, force feedback is more important because of the risk to bend or break the delicate needle. Indeed, to make an anastomosis on vessels under 1 mm diameter, the surgeon needs a needle with a diameter below 50 $\mu$m (needle reference 11/0 or lower).

### *2.5 Instrument exchange*

The surgeon uses different types of instruments according his/her habits. The more usual instruments are a clamp-gripper for the clamp, micro-scissors to cut vessel and thread, a curved or straight micro-gripper and/or a needle holder to handle the vessels and the needle. The mean time of instrument exchange is 6 s and the maximum acceptable exchange is 10 s (data come from analysis of a microanastomoses during DIEP procedure).

To sum up, the requirements of the ASTEMA are:

- a bimanual instruments holder,
- a design suited to the microsurgical environment with a microscope,
- a positioning accuracy of 10 $\mu$m,
- a force capacity of more than 2 N,
- a workspace of 40x50x40 mm$^3$ in position and encompassed by the close wrapper of the figure 3 in orientation,
- a speed of 100 mm/s in position, 56 °/s for the transverse angular velocity (velocity without the self-rotation axis) and 700 °/s for the self-rotation

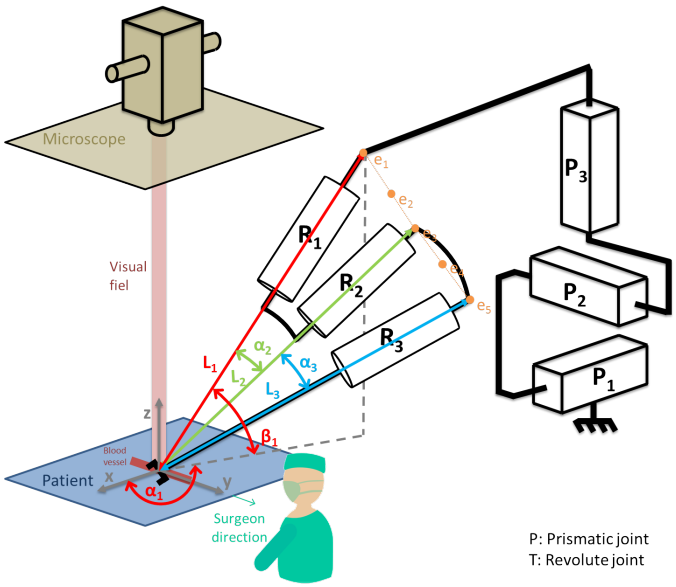


Fig. 5. Robot topology and spherical wrist parameters. The blood vessel is parallel to $y$ axis and the surgeon is in $y > 0$ and $x = 0$. The environment is represented by two planes for the patient and the microscope and one cylinder for the surgeon's visual field. Points $e_1$, $e_2$, $e_3$, $e_4$ and $e_5$ form the robot's shape. Scale is not respected for scheme legibility.

axis angular velocity. These speeds include 99.9% of data [Vanthournhout et al. (2015a)],
- no force feedback except the clamping force feedback,
- a possibility to change the instruments in maximum 10 s,

## 3. IMPLEMENTATION

The ASTEMA is a bimanual telerobotic system designed for one surgeon. In a first step, we developed a prototype of the right hand device that should comply with the above requirements.

### *3.1 Topology*

The robot needs six degrees of freedom for controlling instrument position and orientation. So the topology chosen is a classical decoupled structure with a remote center of movement (RCM) [Mitsuishi et al. (2013); Miroir et al. (2012)]. It includes three linear positioning tables with high accuracy ($\pm 1$ $\mu$m) and a high-stiffness spherical wrist with the last motorized axis coinciding with the instrument axis as shown in figure 5. The instrument tip is on the RCM. So in theory, the positioning and the orientation are decoupled and the accuracy of the linear tables motion is directly the accuracy of the instrument tip linear motion.

### *3.2 Optimization of the wrist geometrical parameters*

A dimensional optimization of the wrist was carried out regarding the constraints of workspace (attainable orientations) and avoidance of collisions with the environment close to the anastomosis (the patient and the microscope). The dimensions of the linear actuators were chosen to encompass the entire workspace required, this portion of the robot being at a certain distance from the anastomosis and thus only slightly constrained in terms of size.

The spherical wrist topology is defined by 7 parameters as shown in figure 5:

- $\alpha_1$, $\beta_1$ define the orientation of the first wrist axis with respect to the coordinate system aligned with the linear axis,
- $\alpha_2$ is the angle between the first and the second wrist axis
- $\alpha_3$ is the angle between the second and the third wrist axis
- $L_1$, $L_2$ and $L_3$ are the distances between the instrument tip and the furthest physical point of the robot along its revolute axis 1, 2 and 3 respectively. These parameters do not come in play in the wrist geometric model but characterize its maximal physical envelope. In particular, these distances depend on the location of the 3 motors along the wrist axis.

The 7 parameters were optimized according to 3 constraints and 2 objectives:

- Constraints
  - Reach all the measured workspace
  - Do not collide with the environment (microscope, patient and left robot)
  - Do not pass in the surgeon's visual field
- Objectives
  - Evaluation of the dexterity ($dext = \sigma_{min}/\sigma_{max}$ with $\sigma_{min}$ and $\sigma_{max}$ the minimum and maximum eigenvalue of the jacobian)
  - Evaluation of the distance between the robot and the environment (minimum distance between the robot's wrapper ($e_1$ to $e_5$) and the microscope, patient and visual field planes and cylinder).

The optimization was based on a systematic exploration of all parameters (cover method). Each parameter range was restricted by an inferior and a superior value, discretized by small steps and all possible solutions were tested (see table 1). If a candidate did not fulfill the constraints, it was rejected. If it did, it was classified according to the 2 objectives of dexterity and distance to obstacles. Several exploration stages were carried out, starting by a global exploration with large ranges and rough intervals and then by focusing the exploration with smaller ranges surrounding the best candidates of the previous stage and finer intervals. The final parameters are $L_1 = 190$mm, $\alpha_1 = 240°$, $\beta_1 = 58°$, $L_2 = 210$mm, $\alpha_2 = 46°$, $L_3 = 160$mm and $\alpha_3 = 45°$. More pieces of information about this optimization can be found in [Vanthournhout et al. (2015a)].

### *3.3 Geometric and dynamic models*

In such a kinematic structure, position of the instrument tip and orientation of the instrument can be controlled in a decoupled manner by the actuators of the linear tables and of the wrist respectively. Therefore the geometric models of the linear tables and of the wrist were derived independently and take the form of a position transformation matrix and of an orientation transformation matrix respectively. So by combination, the global geometric model is computed as a transformation matrix $R_G$:

Table 1. Parameter discretisation during optimization. Come from [Vanthournhout et al. (2015a)].

| | First optimization: large range and rough interval | | | Final optimization: small range and fine interval | | |
|---|---|---|---|---|---|---|
| | Min | Step | Max | Min | Step | Max |
| $L_1$ [mm] | 100 | 20 | 220 | 175 | 5 | 230 |
| $\alpha_1$[o] | -80 | 2 | 80 | -68 | 1 | -56 |
| $\beta_1$[o] | 40 | 2 | 80 | 51 | 1 | 61 |
| $L_2$ [mm] | 100 | 20 | 220 | 150 | 5 | 230 |
| $\alpha_2$[o] | 20 | 2 | 60 | 45 | 1 | 50 |
| $L_3$ [mm] | 100 | 20 | 220 | 90 | 5 | 190 |
| $\alpha_3$[o] | 20 | 2 | 60 | 42 | 1 | 53 |

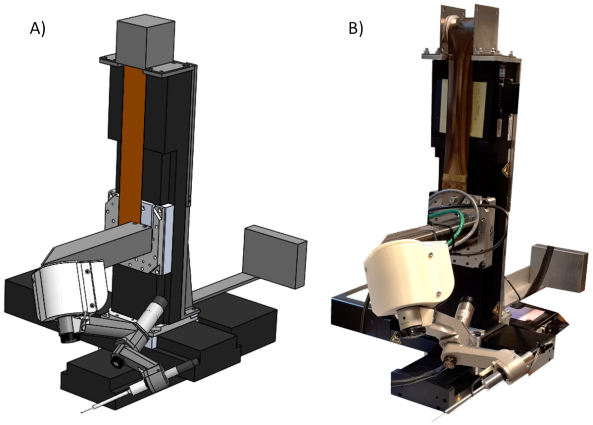


Fig. 6. A) CAO representation of robot. B) Real robot.

$$R_G = R_P(x_p, y_p, z_p)\ R_O(\gamma_1, \gamma_2, \gamma_3) \quad (1)$$

With $R_P$ the position transformation matrix, $R_O$ the orientation transformation matrix, ($x_p$, $y_p$, $z_p$) the positions of each linear table and ($\gamma_1$,$\gamma_2$,$\gamma_3$) the angles of each rotation axis in the wrist.

The linear table model is defined directly by

$$R_P = Tr(x, x_p)\ Tr(y, y_p)\ Tr(z, z_p) \quad (2)$$

with $Tr(i, j)$, the pure translation transformation matrix along axis $i$ of a distance $j$. The orientation transformation matrix is:

$$R_O = Rot(z, \pi/2 + \alpha_1)\ Rot(x, -(\pi/2 + \beta_1)\ Rot(z, \gamma_1) * Rot(x, \alpha_2)\ Rot(z, \gamma_2)\ Rot(x, \alpha_3)\ Rot(z, \gamma_3) \quad (3)$$

with $Rot(i, j)$, the pure rotation transformation matrix around axis $i$ of the angle $j$. $R_P$ and $R_O$ are kept as matrix multiplication for readability.

A dynamic model was developed with a symbolic software to model and analyze multibody systems [Fisette (2017)]. It allowed us to compute the required motor torques taking into account the axes weights and the needed instrument acceleration when the maximum angular acceleration and speed are imposed in all directions, in each point of the angular workspace. So the transmitted torque for rotary actuators 1 and 2 must be at least 320 mNm (1130 mNm in peak) and 145 mNm (150 mNm in peak) respectively. The torque for rotary actuator 3 is not significant because the robot instrument is aligned with its axis and has low rotational inertia and external load.

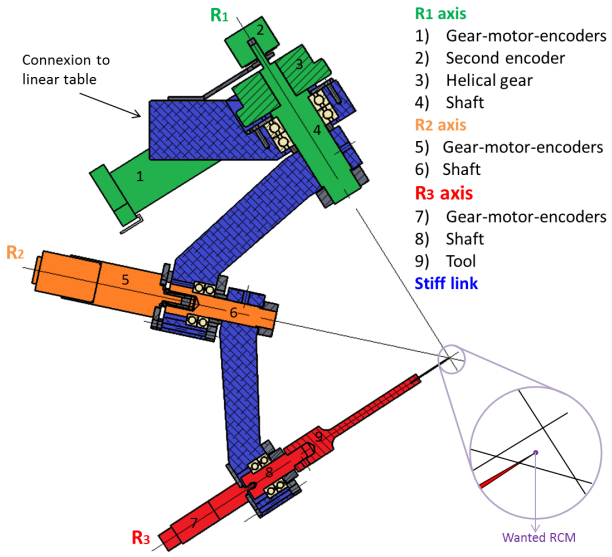


Fig. 7. Spherical wrist cross-section of robot. Real RCM does not exist due to manufacturing tolerance, free-play and flexibility.

### *3.4 Detailed design*

The ASTEMA robot is shown in figure 6. It is composed of three perpendicular linear tables with high resolution followed by a home-made spherical wrist with optimized dimensions.

The linear tables (Newport ILS100-CC) are taken away from the surgical area using a stiff link tothe spherical wrist. These linear tables offer a range of motion of 100 mm and a resolution of 1 $\mu$m. Because the surgeon is in the loop of teleoperation, the resolution is more important than the accuracy of the robot. The range of motion is wider than the specified linear workspace and will allow to test several strategies to scale down the movement with a larger workspace.

The spherical wrist details are shown in figure 7. A particular attention was given to alignment between actuators shafts and expected RCM. First, a DC gear-motor (2657W012CR 23:1, Faulhaber, Schönaich, Germany) is mounted perpendicularly to the $R_1$ axis. The movement is transmitted to the $R_1$ axis by a helical gear (20:38) and a high-resolution encoder (SCA24, 7500 pulses/revolution, Scancon, Hilleroed, Denmark) is mounted on the top of the $R_1$ axis (in green). Axes $R_2$ and $R_3$ (in orange and red in figure 7) are actuated by DC motors with backlash-free planetary gearboxes and with standard encoders (2232R012SR 69.2:1 IE2-1024 and 1224E012S 69.2:1 HEM3-256-W, Faulhaber, Schönaich, Germany). The $R_1$ axis is different from $R_2$ and $R_3$ because there is not Faulhaber backlash-free gearboxes allowing enough torque for the $R_1$ joint. This assembly allow to know precisely the angular position in order to compensate possible error in position with a calibration.

The links between joints (in blue in figure 7) are made of stainless steel for the $R_1$ axis and of aluminium alloy for $R_2$ and $R_3$ and were machined in one piece. Super-

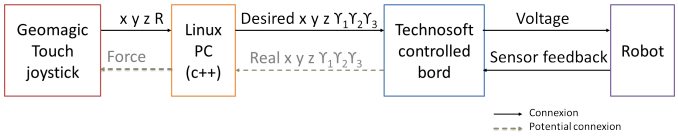


Fig. 8. Robot control diagram. Real position and orientation are used for RCM compensation only when it is tested. Forces are sent to joystick only to limit the workspace.

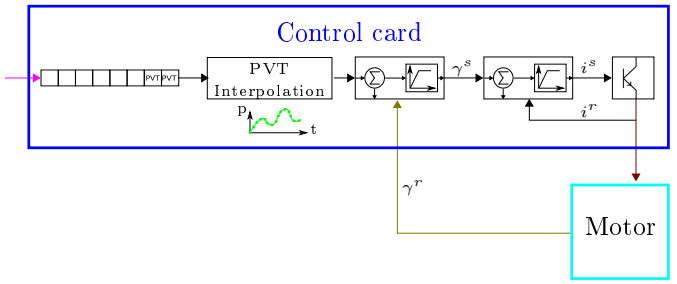


Fig. 9. Internal operations of the control cards.

precision angular contact ball bearings (71900, 71901 and 71904 ACD/P4ADGB, SKF, Sweden, Goteborg) are used and the coupling between gears and actuators shafts are rigid. All these precautions allow to have a good rigidity, little play and so to minimize sources of imprecision.

Currently the robot is simply placed on a table as it could be in experimental surgery. In the operating room, it will be attached directly to the microscope. So the ASTEMA could therefore be installed at the same time as the microscope and be easily moved during operation if there are several microsurgery sites on the patient.

### *3.5 Control*

The robot is teleoperated with a six degrees of freedom GeomagicTouch joystick (resolution: 55 $\mu$m, see joystick in figure 10) through a computer running on Linux with a C++ code and interfaced with Technosoft control boards for low-level regulation of the actuators. The robot control diagram is shown in figure 8.

The Technosoft control cards (IPOS 3602 SX and IPOS 3604 SY, Technosoft, Neuchâtel, Switzerland) use the PVT control mode (Point-Velocity-Time). At each instant t, the computer sends to the cards a time, a position and a speed that the engine must reach. The card stores the data sent in a reception buffer, interpolates the desired positions to order 3 and controls the motors in position. The buffer is emptied as the points are executed. The controller consists of a position loop (PID controller - Proportional, Integral, Derivative) superimposed on a current loop (PI or I controller). Figure 9 shows the internal operation of the control cards.

### *3.6 Correction of the wrist geometric model*

Despite all precautions taken, the actual robot geometric model shows discrepancies with respect to the theoretical model developed in section 3.3, mainly because of machining tolerance. In particular, a coupling between instrument rotation and instrument tip displacement appears since the wrist axes are not perfectly aligned with the instrument tip. Practically, when the instrument orientation is modified through actuation of the robot wrist, the tip position moves at the same time.

To highlight these model discrepancies, errors between theoretical and actual instrument tip positions for 30 different desired instrument orientations were measured using a microscope with camcorder and a x40 optical magnification as shown in figure 10. The picture resolution is 6.2 $\mu$m/px and a shape recognition algorithm (using the `bwtraceboundary` function of Matlab, based on Moore-Neighbor tracing algorithm) was used to locate the needle tip. The desired angle to each axis to obtain the 30 different instrument orientations were:

$$[\gamma_1\ \gamma_2\ \gamma_3] = \begin{bmatrix} 0:10:90 & 90 & 360 \\ 45 & 90 & 360 \\ 0 & 90:10:150 & 360 \end{bmatrix}^\circ$$

The maximum error between desired and obtained positions is 307 $\mu$m as shown in figure 11.

In order to compensate for these errors, a modified wrist geometric model was defined. It includes 16 corrective parameters with constant values to be identified. Here is the new wrist orientation model:

$$\begin{aligned} R_O = {} & Rz(\alpha_1 + \pi/2 + p_1) * Rx(-\beta_1 - \pi/2 + p_2) \\ & * Tz(-L_1 + p_3) * Tx(p_4) * Ty(p_5) * Rz(\gamma_1 + p_6) \\ & * Tz(L_1) * Rx(\alpha_2) * Tz(-L_2) \\ & * Rx(p_7) * Tx(p_8) * Tz(p_9) * Rz(\gamma_2 + p_{10}) \\ & * Tz(L_2) * Rx(\alpha_3) * Tz(-L_3) \\ & * Rx(p_{11}) * Tx(p_{12}) * Tz(p_{13}) * Rz(\gamma_3 + p_{14}) \\ & * Tz(L_3 + p_{15}) * Tx(p_{16}) \end{aligned} \quad (4)$$

with $p_i$ the corrective parameter number i. Because the absolute height is not measured by the camera which is placed vertically, the parameter $p_3$ could not be identified and was fixed to 0. Indeed, it does not affect the model because the delta of height is fixed whatever the angular movement is.

To identify the set of corrective parameters, an optimization program relying on a `lsqnonlin` function of Matlab, based on "trust-region-reflective" algorithm was used.

The theoretical remaining maximum error after model correction is 18$\mu$m and is shown in figure 11. This remaining error may come from measurement inaccuracies and variable plays in the robot joints that can not be identified and were not compensated through the modified model.

The efficiency of the RCM compensation was tested on a real trajectory. Results are shown in figure 12 for $\gamma_1$ and $\gamma_2$. Before the RCM calibration, the maximum error is 393 $\mu$m and after the calibration it is 127 $\mu$m. So the precision was increased by a factor 3. Besides, one can see that error increases as the instrument goes further away from the central axis of the angular workspace. This can be explained by the fact that the parameters identification reported above was based on a relatively localized set of angular configurations that were chosen near the central axis of the angular workspace, where

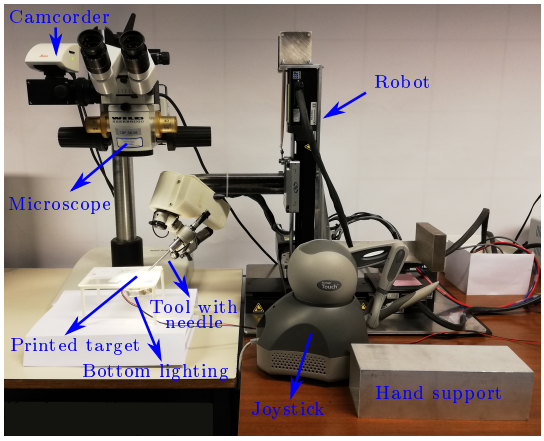


Fig. 10. Calibration and experiment setup.

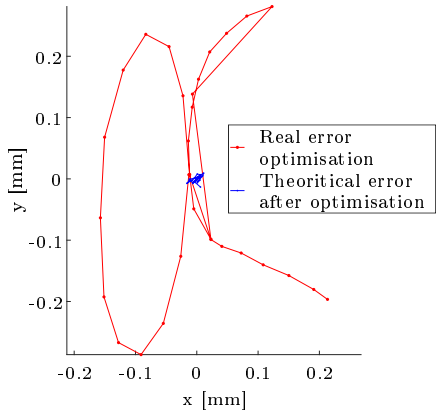


Fig. 11. Error between desired and obtained positions before (maximum error: 307 $\mu$m) and after (maximum error: 18 $\mu$m) the model optimization.

the angular configurations adopted during an anastomosis are mainly located. In this narrow angular region, the maximum error is 222 $\mu$m without RCM compensation and 36 $\mu$m with RCM compensation (error divided by a factor 6).

Regarding the calibration of axis 3 ($\gamma_3$), results are depicted in figure 13. Before and after RCM compensation introduction, the maximum errors are 274 $\mu$m and 22 $\mu$m respectively. So the error is divided by a factor 12 when the compensation is added.

In the central area of the workspace, when the two independent errors are combined, it gives a total error of 496 $\mu$m without RCM compensation and 58 $\mu$m with RCM compensation.

## 4. EXPERIMENTAL PERFORMANCE ASSESSMENT

This section is dedicated to the ASTEMA performance evaluation. Two experiments were performed to show the ASTEMA performance with and without subjects in the control loop and to check whether RCM compensation helps the subject during a teleoperation task. The first experiment allows to analyse the error with a simple positioning trajectory and the second with a complex angular trajectory.

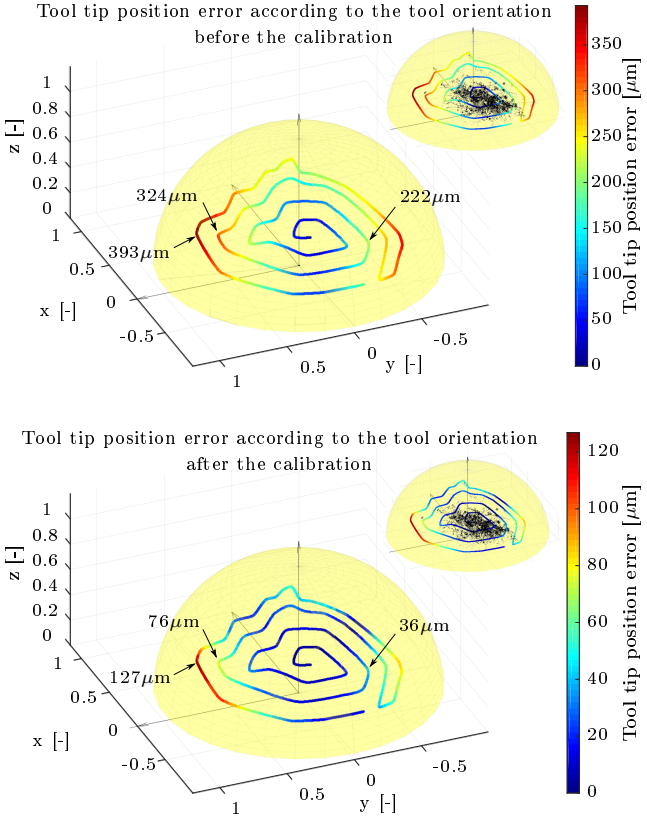


Fig. 12. Instrument tip position error according to the orientation before and after calibration during an angular trajectory which wanders the wanted workspace ($\gamma_1$ and $\gamma_2$ movement). The angular position is represented by points which correspond to the intersection between a sphere center on the instrument tip with a dimensionless radius of 1 and the instrument, as shown in figure 3. In the top right-hand corners, the black point are the orientation measured during a microanastomosis in the needs analysis (see section 2).

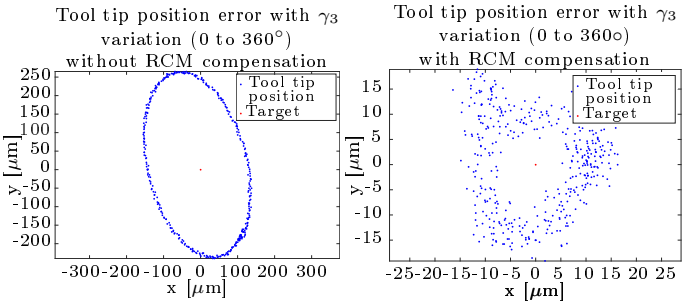


Fig. 13. Instrument tip position error before and after calibration during a self rotation of axis 3 of 360° ($\gamma_3$ movement).

### *4.1 Setup*

Almost the same setup as for the model correction in section 3.6 is used here. The camcorder records a needle attached to the robot instrument at 30 Hz across the microscope with a x40 optical magnification. A trajectory to follow is printed in magenta on white paper with high resolution (1200 dpi) and the light comes from the bottom across the paper to avoid shadows as shown in figure 10. The desired position in $z$ is defined in the robot high-level

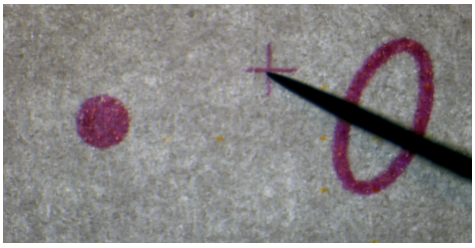

Fig. 14. Trajectory printed and needle.

controller and on the joystick by a physical force imposed by the joystick itself. During the experiments, subjects had to watch in the microscope with one eye only to see the trajectory always in the same place. Subjects had to rest their forearm and wrist on a support.

A subject had to follow a desired trajectory with the needle tip while the ASTEMA system was providing a downscaling factor of 30 between the subject gestures and the needle tip linear movements. Because the joystick resolution is 55 $\mu$m, the scale factor of 30 leads to a needle-tip linear movement resolution of 1.8 $\mu$m.

The printed trajectory are shown in figure 14. In experiment 1, the desired trajectory was a circle of 1 mm diameter to be followed by the needle tip with a free needle orientation. This enabled us to assess the ASTEMA performance when precise linear movements are mainly used. In the experiment 2, the desired trajectory was an angular trajectory with a fixed needle tip position. Our aim here was to measure the ASTEMA performance when a complex angular trajectory is generated with a precise positioning of the needle tip. The angular trajectory in experiment 3 was based on a cross mark and an ellipse. Subjects had to maintain the needle tip at the cross center and to move the needle orientation while following the elliptic trajectory with a specific point on the needle shaft. Subjects were asked to focus on the tip positioning precision and not on the execution speed or the orientation precision.

Each test was performed under different conditions: with RCM compensation, without RCM compensation, and without ASTEMA (by hand). Besides, the circle test in experiment 1 was also made with and without fixed orientation of the needle. $[\gamma_1\ \gamma_2\ \gamma_3] = [40\ 115\ 20]^\circ$ was selected as fixed orientation to preserve a good vision of the instrument tip. In each case, the joystick orientation remained free. A different order among these conditions was used for each subject (all combinations were tested) and the subjects ignored the condition being tested. A given subject had to perform three paths around the circle and three two-way angular trajectories for each possible condition. One minute training was scheduled before each experiment.

Four subjects with an engineering background and without any experience in microsurgery or with the ASTEMA robot took part in these experiments. Additionnaly, each experiment was also performed autonomously by the ASTEMA robot without any subject within the control loop. As the angular trajectory was not totally fixed, it was chosen after analysis of the angular trajectory of the four subjects, in order to be the closest from their average trajectory.

A statistical study was executed. A linear model followed by a Tukey test was used to highlight differences between the tested modes (significant test if p value $> 5$ %).

### *4.2 Results and discussion*

*Experiment 1* Figure 15 gives examples of circular trajectories followed during the first experiment. Figure 16 shows the mean values of error for all subjects and for the autonomous controller (PC). The statistic study shows that subjects are significantly better with the robot than by hand but the tested groups with the robot are not significantly different each other. A summary of the best performance of subjects with and without the ASTEMA robot is reported in table 2.

As expected, the mean error of the autonomous controller is larger without RCM compensation (47 $\mu$m). With the RCM compensation the mean error is of 9 $\mu$m and with fixed orientation of 2.5 $\mu$m which is under the precision of measure ($\sim$6.4 $\mu$m).

In figure 15, the positive effect of the assistance offered by the ASTEMA robot is clearly visible in comparison to the trajectory without the robot help. All subjects perform better with the ASTEMA assistance by a factor 4 approximatively. Currently, the mean precision of the best subject is 14 $\mu$m and the robot with an autonomous controller has a precision of 9 $\mu$m. It is close to the 10 $\mu$m desired precision identified in section 2.2.

So, currently subjects induce errors bigger than the autonomous controller alone even when the orientation is fixed and that there is no error coming from spherical wrist. Indeed, teleoperation induces additional errors due to the limited dexterity of the subject, the manipulability of the joystick or the optical zoom limitation. With a bigger optical zoom and scale factor, subjects could certainly reach the robot accuracy if necessary.

On the other hand, without RCM compensation, the mean error is lower for a subject than for the autonomous controller. This is most probably due to the ability of subjects to compensate for these coupled motions thanks to real-time and high-quality visual feedback from the magnified microscope view. However, special attention should be paid to not increase the surgeon mental load because of this instinctive compensation.

Additionally, it can be observed that the time taken to cover the trajectory is always shorter by hand than with robotic assistance (between 13 s and 18 s by hand and between 35 s and 70 s with robotic assistance depending on the subject). This can be explained obviously by the fact that the large downscaling of joystick motions significantly reduces instrument tip velocity, thus increasing the time required to follow a defined path.

*Experiment 2* Figure 17 gives an example of instrument tip position during an angular trajectory. Figure 18 shows the mean values of error for all subjects and for a trajectory controlled by PC. The statistic study shows that subjects are significantly better with the robot than by hand but

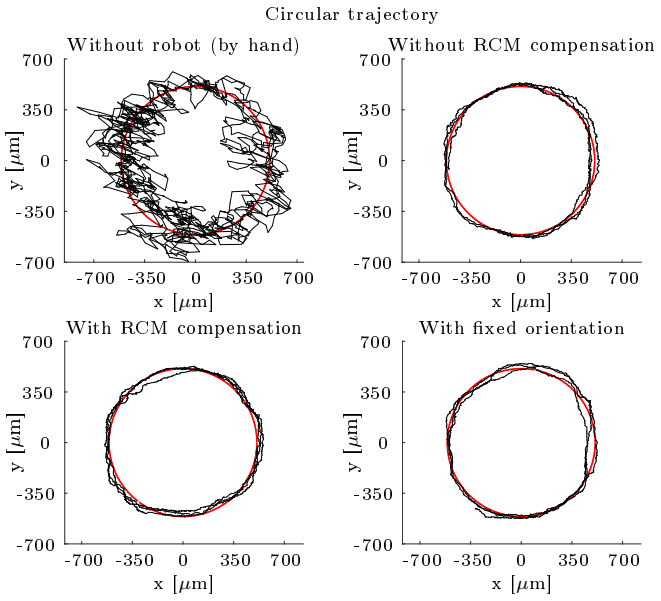


Fig. 15. Instrument tip position followed by subject 2 when following a circular trajectory of 1 mm diameter.

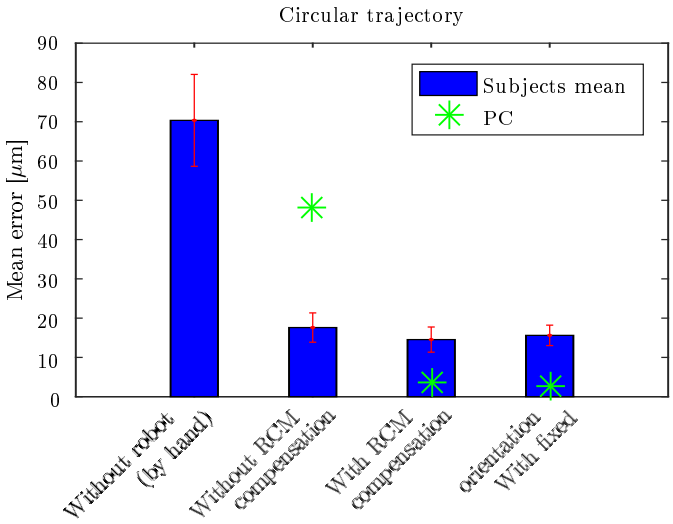


Fig. 16. Mean error in instrument tip position during a circular trajectory (experiment 1).

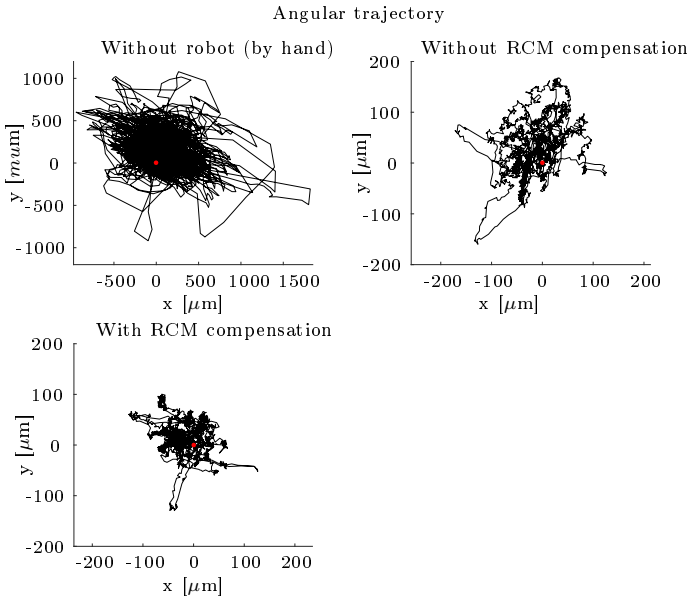


Fig. 17. Instrument tip position of subject 2 when following the angular trajectory and keeping the tip fixed.

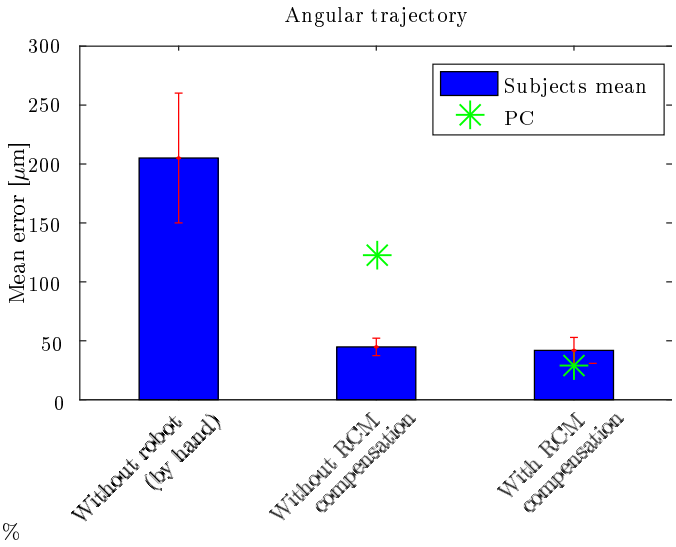


Fig. 18. Mean error in instrument tip position during an angular trajectory with a fixed desired position (experiment 2).

the tested groups with the robot are not significantly different each other.

Accuracy is improved by a factor 4 to 7 from hand execution to teleoperation with the ASTEMA system. In addition, the time required to perform the task is shorter with the robot than by hand (between 13 s and 18 s with robot and between 80 s an 268 s by hand depending on the subject). Moreover, subjects' mean errors with ASTEMA are 2 to 3 times lower than mean error obtained during automatic trajectory execution by the PC. These results confirm the interest of using the ASTEMA teleoperated system for microanastomosis.

When the RCM compensation is applied, the mean error of autonomous controller is significantly reduced (23 $\mu$m compared to 222 $\mu$m). This proves again the effectiveness of the RCM compensation. However, the RCM compensation seems have no visible effect on the precision of subjects (75 $\mu$m without compensation, compared to 62 $\mu$m with compensation). This tends to show again that subjects compensate by themself a large part of the error due to coupling between position and orientation when an imperfect RCM is implemented.

In the trajectory prescribed in this experiment, the instrument makes an angular diplacement of more than 65°. This trajectory thus evolves in the outer portion of the angular workspace identified in section 2.1. With an average accuracy of 45 $\mu$m for the best subject, the accuracy specification of 100 $\mu$m established in section 2.2 for large angulations is therefore fulfilled.

Table 2. ASTEMA performance

| **Error mean** [$\mu$m] | Without robot (by hand) | Without RCM compensation | With RCM compensation | With fixed orientation |
|---|---|---|---|---|
| Sujets' best circular trajectory | 75 | 18.5 | 14 | 18 |
| Autonomous circular trajectory | N.A. | 46 | 9 | 2.5 |
| Sujets' best angular trajectory | 271 | 59.5 | 45 | N.A. |
| Autonomous angular trajectory | N.A. | 222 | 22.5 | N.A. |

## 5. CONCLUSION AND PERSPECTIVE

Microanastomosis is a complex task that requires precision and dexterity. Under 1 mm diameter, only experimented surgeons can perform this gesture safely. We designed and built a novel telerobotic assistant, called ASTEMA. It has a resolution under 1 $\mu$m, a precision of 9 $\mu$m along a trajectory under autonomous control, and an average error of 14 $\mu$m during a circular trajectory controlled by a subject. According to these experimental results, our system will eventually increase the precision of the surgeon and allow to move from microsurgery to supermicrosurgery.

The table 3 allows to compare the ASTEMA with the need defined in section 2 and with some of the most relevant and sufficiently documented robots of the state of the art. ASTEMA meets the needs of microanastomosis particularly well in terms of precision, workspace and speed. When compared to other robots, we can see that it has a greater or equal accuracy and this especially compared to the da Vinci which is the main marketed robot for microanastomosis. This is due to its kinematics which allows to be intrinsically accurate because it directly transfer the high resolution of the linear table to the tip of the tool. ASTEMA also allows a speed identical to the surgeon's movements, which is not the case of other robots and which will reduce partly the operating time during a microanastomosis.

Yet, these first experiments also highlighted a trend to slow down instruments motions through teleoperation, due to the high downscaling factor used. The next step will consist in trying to solve this common speed/accuracy trade-off that all existing telesurgery systems face currently. Adaptive downscaling strategies are being envisioned and implemented, based for instance on the instrument position with respect to the microanastomosis site or on the velocity of the master joystick [Conti and Khatib (2005); Dubey et al. (2001); Munoz et al. (2011); Ko et al. (2017)]. Indeed, the anastomose seems to be particularly adapted to these strategies because it need to realize small, slow and precise gestures, for example to insert the needle in the vessel and, big, quick, not too precise gestures for example to make a knot or pull on the thread. An experimental comparison of several adaptive strategies will then be carried out with surgeons, trying to identify the most suitable strategy in terms of usability, accuracy when/where needed and task duration.

Finally, a motorised tools and a mirror robot for the left instrument is currently being built. With a fully operational bi-manual device, we will be able to move on to more realistic experiments involving actual microanastomosis gestures.


## ACKNOWLEDGEMENTS

The authors would like to thank the reconstructive microsurgery team of Cliniques universitaires Saint-Luc for their advices during the needs analysis and experiments. Authors are also grateful to Prof. Gianello and his team from Experimental Surgery Laboratory (Institute of Experimental and Clinical Research, UCLouvain), Prof. Dehoux, and all colleagues from iMMC and ISIR for their help and support in this project. The authors also thank the interns Quentin Panissod and Valentin Rebiere for their respective contributions on the studies of the influence of backlashes and the calibration of ASTEMA.


## REFERENCES


Cau, R., Schoenmakers, F., Steinbuch, M., van Mulken, T., and van der Hulst, R. (2014). Design and preliminary test results of a novel microsurgical telemanipulator system. In *5th IEEE RAS/EMBS International Conference on Biomedical Robotics and Biomechatronics*, 352–356. IEEE.

Cau, R. (2014). *Design and Realization of a Master-Slave System for Reconstructive Microsurgery*. Ph.D. thesis, Eindhoven University of Technology.

Charles, S., Das, H., Ohm, T., Boswell, C., Rodriguez, G., Steele, R., and Istrate, D. (1997). Dexterity-enhanced telerobotic microsurgery. In *Advanced Robotics, 1997. ICAR'97. Proceedings., 8th International Conference on*, 5–10. IEEE.

Conti, F. and Khatib, O. (2005). Spanning large workspaces using small haptic devices. In *First Joint Eurohaptics Conference and Symposium on Haptic Interfaces for Virtual Environment and Teleoperator Systems. World Haptics Conference*, 183–188. IEEE.

Dubey, R.V., Everett, S., Pernalete, N., and Manocha, K.A. (2001). Teleoperation assistance through variable velocity mapping. *IEEE Transactions on Robotics and Automation*, 17(5), 761–766.

Fisette, P. (2017). Robotran: Symbolic generator of multibody systems. `www.robotran.be`.

Huart, A., Facca, S., Lebailly, F., Garcia, J.C., and Liverneaux, P.A. (2012). Are pedicled flaps feasible in robotic surgery? report of an anatomical study of the kite flap in conventional surgery versus robotic surgery. *Surgical innovation*, 19(1), 89–92.

Katz, R., Rosson, G., Taylor, J., and Singh, N. (2005). Robotics in microsurgery: use of a surgical robot to perform a free flap in a pig. *Microsurgery*, 25(7), 566–569.

Ko, S., Nakazawa, A., Kurose, Y., Harada, K., Mitsuishi, M., Sora, S., Shono, N., Nakatomi, H., Saito, N., and Morita, A. (2017). Intelligent control of neurosurgical robot mm-3 using dynamic motion scaling. *Neurosurgical focus*, 42(5), E5.

Le Roux, P., Das, H., Esquenazi, S., and Kelly, J. (2001). Robot-assisted microsurgery: a feasibility study in the rat. *Neurosurgery*, 48(3), 584–589.

Liverneaux, P., Berner, S., Bednar, M., Parekattil, S., Ruggiero, G., and Selber, J. (2013). *Telemicrosurgery: robot assisted microsurgery*. Springer. doi:10.1007/978-2-8178-0391-3.

Miroir, M., Nguyen, Y., Szewczyk, J., Sterkers, O., and Grayeli, A. (2012). Design, kinematic optimization,

Table 3. Comparative between ASTEMA, the need and robots the most pertinent and sufficiently documented in reconstructive microsurgery.

| | Accuracy [$\mu$m] | Workspace [cm$^3$] | Speed [mm/s] | Volume | University/company | Reference |
|---|---|---|---|---|---|---|
| ASTEMA | 9-22 | 1000 | 100 | ++ | Université catholique de Louvain | Vanthournhout et al. (2014)<br>Vanthournhout et al. (2015b)<br>Vanthournhout et al. (2016) |
| Da Vinci | <1000 | 6250 | | - - - | Intuitive Surgical | Katz et al. (2005)<br>Huart et al. (2012)<br>Liverneaux et al. (2013)<br>Saleh et al. (2015)<br>Willems et al. (2016) |
| RAMS | 10-25 | 400 | | ++ | JPL-Caltech | Schenker (1995)<br>Charles et al. (1997)<br>Saraf (2008) |
| MSR | 30-40 | 6.3 | 10 | + | Eindhoven University of Technology Microsure | Cau et al. (2014)<br>van Mulken et al. (2018b)<br>van Mulken et al. (2018a) |
| MM-3 | 44 | 3400 | 50 | - - | Université de Tokyo | Morita et al. (2005)<br>Mitsuishi et al. (2013) |
| Besoin | 10-100 | 100 | 100 | ++ | | |


and evaluation of a teleoperated system for middle ear microsurgery. *The Scientific World Journal*, 2012. doi: 10.1100/2012/907372.

Mitsuishi, M., Morita, A., Sugita, N., Sora, S., Mochizuki, R., Tanimoto, K., Baek, Y., Takahashi, H., and Harada, K. (2013). Master-slave robotic platform and its feasibility study for micro-neurosurgery. *Int J Med Robot Comput Assist Surg*, 9(2), 180–189.

Mitsuishi, M., Watanabe, H., Nakanishi, H., Kubota, H., and Iizuka, Y. (1997). Dexterity enhancement for a telemicro-surgery system with multiple macro-micro colocated operation point manipulators and understanding of the operator's intention. In *CVRMed-MRCAS'97*, 821–830. Springer.

Morita, A., Sora, S., Mitsuishi, M., Warisawa, S., Suruman, K., Asai, D., Arata, J., Baba, S., Takahashi, H., Mochizuki, R., et al. (2005). Microsurgical robotic system for the deep surgical field: development of a prototype and feasibility studies in animal and cadaveric models. *Journal of neurosurgery*, 103(2), 320–327.

Munoz, L.M., Casals, A., Frigola, M., and Amat, J. (2011). Motor-model-based dynamic scaling in human–computer interfaces. *IEEE Transactions on Systems, Man, and Cybernetics, Part B (Cybernetics)*, 41(2), 435–447.

Panchulidze, I., Berner, S., Mantovani, G., and Liverneaux, P. (2011). Is haptic feedback necessary to microsurgical suturing? comparative study of 9/0 and 10/0 knot tying operated by 24 surgeons. *Hand Surgery*, 16(1), 1–3.

Safwat, B., Su, E., Gassert, R., Teo, C., and Burdet, E. (2009). The role of posture, magnification, and grip force on microscopic accuracy. *Ann Biomed Eng*, 37(5), 997–1006.

Saleh, D., Syed, M., Kulendren, D., Ramakrishnan, V., and Liverneaux, P. (2015). Plastic and reconstructive robotic microsurgery–a review of current practices. In *Annales de Chirurgie Plastique Esthétique*, volume 60, 305–312. Elsevier.

Saraf, S. (2008). Robotic assisted microsurgery (rams): application in plastic surgery. In *Medical Robotics*. InTech.

Schenker, P.S. (1995). Development of a telemanipulator for dexterity enhanced microsurgery. *MRCAS'95*, 81–88.

Shaw, W., Ko, C., Ahn, C., and Markowitz, B. (1996). Safe ischemia time in free-flap surgery: a clinical study of contact-surface cooling. *Journal of reconstructive microsurgery*, 12(7), 421–424.

Taleb, C., Nectoux, E., and Liverneaux, P. (2008). Telemicrosurgery: a feasibility study in a rat model. *Chirurgie de la main*, 27(2-3), 104–108.

van Mulken, T.J., Boymans, C.A., Schols, R.M., Cau, R., Schoenmakers, F.B., Hoekstra, L.T., Qiu, S.S., Selber, J.C., and van der Hulst, R.R. (2018a). Preclinical experience using a new robotic system created for microsurgery. *Plastic and reconstructive surgery*.

van Mulken, T.J., Schols, R.M., Qiu, S.S., Brouwers, K., Hoekstra, L.T., Booi, D.I., Cau, R., Schoenmakers, F., Scharmga, A.M., and van der Hulst, R.R. (2018b). Robotic (super) microsurgery: Feasibility of a new master-slave platform in an in vivo animal model and future directions. *Journal of surgical oncology*.

Vanthournhout, L., Herman, B., Duisit, J., Château, F., Szewczyk, J., Lengelé, B., and Raucent, B. (2015a). Requirements analysis and preliminary design of a robotic assistant for reconstructive microsurgery. In *Engineering in Medicine and Biology Society (EMBC), 2015 37th Annual International Conference of the IEEE*, 4926–4930. IEEE.

Vanthournhout, L., Herman, B., Duisit, J., Château, F., Szewczyk, J., Lengelé, B., and Raucent, B. (2015b). Requirements analysis and preliminary design of a robotic assistant for reconstructive microsurgery. In *2015 37th Annual International Conference of the IEEE Engineering in Medicine and Biology Society (EMBC)*, 4926–4930. IEEE.

Vanthournhout, L., Herman, B., Duisit, J., Château, F., Szewczyk, J., Lengelé, B., Raucent, B., et al. (2014). Toward user-friendly robotic assistance for enhancing accuracy and safety of reconstructive microsurgery. In *4th Joint Workshop on New Technologies for Com-*

*puter/Robot Assisted Surgery.*

Vanthournhout, L., Herman, B., Szewczyk, J., Lengelé, B., and Raucent, B. (2016). Design and prototyping of a robotic assistant for microsurgery. In *6th Joint Workshop on New Technologies for Computer/Robot Assisted Surgery (CRAS2016).*

Veluvolu, K. and Ang, W. (2010). Estimation and filtering of physiological tremor for real-time compensation in surgical robotics applications. *The International Journal of Medical Robotics and Computer Assisted Surgery*, 6(3), 334–342.

Willems, J.I., Shin, A.M., Shin, D.M., Bishop, A.T., and Shin, A.Y. (2016). A comparison of robotically assisted microsurgery versus manual microsurgery in challenging situations. *Plastic and reconstructive surgery*, 137(4), 1317–1324.

**Léna Vanthournhout** is born in 1990. She obtained the Master's Degree in Electro-Mechanical Engineering, professional focus in Mechatronics in 2013. Then, she started a Ph.D. thesis at UCLouvain on the design, prototyping and testing of a robotic assistant for reconstructive microsurgery under the supervison of Prof. Benoît Raucent and Prof. Benoît Herman. She is also teaching assistant in UCLouvain and member of Louvain Bionics.

**Jérôme Szewczyk** received a MS degree in mechanical engineering from University of Compiègne (France) in 1994 and a PhD degree in robotics at University of Paris VI in 1998. He was assistant professor from 2000 to 2010 at University of Versailles and is now full professor at Sorbonne University at the Institut des Systèmes Intelligents et de Robotique. His research activities concern the design of sensors and actuators for meso-robotics based on smart materials and the optimal design of robotic structures for surgical applications.

**Jérôme Duisit** is born in 1979, he graduated from Lyon University as doctor in dental surgery in 2004, then as a medical doctor in 2010 and PhD in 2018 from the UCLouvain under the supervision of Pr B. Lengelé. He specialized in Plastic in Reconstructive Surgery, we a special focus in autologous and tissue-engineered flaps as well as vascularized composite tissue allotransplantation like face transplant.

**Benoît Lengelé** is born in Brussels, in 1962, he is chairman in Human Anatomy at the UCLouvain and the head of the Plastic and Reconstructive Surgery Department at St Luc university Hospital. In his PhD thesis, he studied the neurodevelopmental mechanisms of cephalogenesis. He is involved in the surgical realization of the first human face transplantation carried out in Amiens, France, in 2005. His actual research is focused now on regenerative (micro)surgery. Member of the Royal Belgian Academy of Medicine and of the French Academy of Surgery, he was ennobled in 2009 by H.M. the King of the belgians.

**Benoît Raucent** is a professor at the Louvain School of Engineering of the UCLouvain. His field of research focuses on the mechatronic integrated design of medical devices, and in particular surgical aids. He has coordinated several books on university pedagogy and more specifically on the learning by problem, the project and the new roles of teachers. Since October 2014, he has been president of the Louvain Learning Lab, a UCLouvain service that deals with educational innovation and teacher training.

**Benoît Herman** is born in 1981 in Belgium, he obtained the Mechanical Engineer degree in 2004. He started a Ph.D. thesis at UClouvain and at Université Montpellier 2-CNRS about the realization of an active scope-holder for laparoscopic surgery - the EVOLAP robot. Since 2017, he is Principal Research Logistic Collaborator with the Institute of Mechanics, Materials and Civil Engineering (iMMC) and head of the CREDEM platform. He is also a regular member of Louvain Bionics.